Dynamic reversible disulfide bonds hydrogel of thiolated galactoglucomannan/cellulose nanofibril with self-healing property for protein release

Bi, Hongjie; Zhang, Xue; Wang, Qingbo; Yong, Qiwen; Xu, Wenyang; Xu, Min; Xu, Chunlin; Wang, Xiaoju

Published in:
Industrial Crops and Products

DOI:
https://doi.org/10.1016/j.indcrop.2023.117615

Published: 15/12/2023

Document Version
Final published version

Document License
CC BY

Industrial Crops & Products 206 (2023) 117615

Contents lists available at ScienceDirect

Industrial Crops & Products

journal homepage: www.elsevier.com/locate/indcrop

Dynamic reversible disulfide bonds hydrogel of thiolated galactoglucomannan/cellulose nanofibril with self-healing property for protein release

Hongjie Bi [a,b,1], Xue Zhang [c,1], Qingbo Wang [b], Qiwen Yong [d], Wenyang Xu [b], Min Xu [e], Chunlin Xu [b], Xiaoju Wang [b,c,*]

[a] College of Chemistry and Materials Engineering, Zhejiang A&F University, Hangzhou, China
[b] Laboratory of Natural Materials Technology, Åbo Akademi University, Henrikinkatu 2, Turku FI-20500, Finland
[c] Pharmaceutical Sciences Laboratory, Faculty of Science and Engineering, Åbo Akademi University, Tykistökatu 6A, Turku FI-20520, Finland
[d] Chemical Synthesis and Pollution Control Key Laboratory of Sichuan Province, China West Normal University, Nanchong 637009, China
[e] Key Laboratory of Bio-Based Material Science and Technology (Ministry of Education), Material Science and Engineering College, Northeast Forestry University, Harbin 150040, China

ARTICLE INFO

Keywords:
Thiolated galactoglucomannan
Cellulose nanofibrils
Reversible disulfide bonds
Self-healing
Protein release

ABSTRACT

In the context of sustainability transition to effectively utilize renewable biopolymers in building functional materials, we report a dynamic reversible nanocomposite hydrogel via thiolated galactoglucomannan (GGMSH) and TEMPO-oxidized cellulose nanofibrils (T-CNF) by deploying a UV-triggered thiol-disulfide exchange reaction. By adjusting the compositional content of GGMSH, the viscoelastic properties of the hydrogel precursors are tuneable and the crosslinking degree of disulfide bonds in these hydrogels dictates their mechanical properties upon UV irradiation. The nanocomposite hydrogels of GGMSH/T-CNF demonstrate robust self-healing properties, attributed to the dynamically reversible disulfide bonds and strong hydrogen bonds between T-CNF and GGMSH. For the hydrogel system of GGMSH/T-CNF/bovine serum albumin (BSA), the swelling behaviour of nanocomposite hydrogels largely dominated the release of BSA out of the hydrogels, suppressing the effect of redox-responsive stimuli with the addition of glutathione. Still, the cytotoxicity test proved a low cytotoxicity of the nanocomposite hydrogel and provided promising reference value to exploit this class of natural polymer-based hydrogel systems in biomedical applications.

1. Introduction

Hydrogel nanomaterials are emerging candidates for constructing Extracellular matrix (ECM)-mimicking matrix in in vitro 3D cell culture and tissue engineering as well as for achieving controlled and bioactive delivery functions for a therapeutic purpose (Laurén et al., 2017; Wang et al., 2022a; Wang et al., 2022b; Zini et al., 2021). Cellulose nanofibrils (CNFs) are one of these cytocompatible nanomaterials, which can be prepared from abundant and renewable natural cellulose in highly crystalline structures. CNFs show a fibrous morphology with a high aspect-of-ratio and offer a massive surface area to interface. These nanosized fibrils also possess excellent water-retention capacity thanks to the intrinsic hydrophilicity of cellulose surface (Masruchin et al., 2018; Wang et al., 2022a). Owing to hydrogen bonding, hydrophobic interactions, electrostatic repulsion, etc, an interconnected network of nanosized fibrils is formed through strong physical entanglements, which results CNFs in a mechanically robust gel behavior at low nanofibril consistency less than 1 wt%. For the top-down production of nanofibrillation, the pre-treatment method, e.g. enzymatic degradation or TEMPO-mediated oxidation, largely determines the surface chemistries of the CNFs (Klemm et al., 2011). On this perspective, the surface chemistries (functional groups and surface charges) are key parameters in determining the colloidal status of nanosized fibrils in the pristine gel or when forming a composite hydrogel with other classes of natural polymers, e.g. chitosan, alginate, or gelatin, etc. (Chinga-Carrasco and Syverud, 2014; Deng et al., 2021; Markstedt et al., 2015; Wang et al.,

* Corresponding author at: Laboratory of Natural Materials Technology, Åbo Akademi University, Henrikinkatu 2, Turku FI-20500, Finland.
E-mail address: xwang@abo.fi (X. Wang).
[1] These authors contributed equally to this work.

https://doi.org/10.1016/j.indcrop.2023.117615

Available online 14 October 2023

2022a; Xu et al., 2019a,2019b; You et al., 2021). The large-surface-area characteristic of the nanosized fibrils promotes the interfacing physiochemical interactions between the matrix and the laden bioactive substances (small molecular drug or protein-type biologics). In quite a few peer studies, CNF-based hydrogels have been considered as carrier systems for a controlled release or even on-demand delivery of therapeutics (Paukkonen et al., 2017; Zini et al., 2021). CNF hydrogels allow solid drug crystals to slowly dissolve into the network followed by a subsequent release, thus achieving immediate and sustained drug release (Paukkonen et al., 2017). Recently, Auvinen et al. have also evaluated the release of several types of nanoparticles (micelles, liposomes, and DNA origami) from the CNF hydrogels to correlate the various surface characteristics of these nanosized payloads with their diffusivity in and through the anionic CNF hydrogels (Auvinen et al., 2022). Basti et al. measured the release of silver nitrate disinfectant from the CNF hydrogel, and the results showed a linear relationship between the amount of absorption and the concentration of the drug (Basti et al., 2022). Zong et al. developed a hydrogel with temperature and redox response to control drug delivery (doxorubicin, berberine) by introducing TEMPO-oxidized CNF (T-CNF) and N,N′-bis(acryloyl)cystamine (Zong et al., 2022). These studies highlight the prospects to apply CNF hydrogels in biomedical research as a non-toxic and xeno-free biomaterial platform suitable for long-term delivery of biologics.

For the fabrication of CNF-hydrogel based drug delivery system (DDS), the crosslinking strategy is the core in resulting in a mechanically strong and robust hydrogel in terms of the handleability of the DDS. T-CNFs with surface groups of carboxyl groups can be physically crosslinked by Ca^{2+} ions, which is the most deployed crosslinking mechanism in designing CNF-based hydrogels (Laurén et al., 2017; Liu et al., 2016a, 2016b). Chemical crosslinking strategies provide more stable covalent bonds at the crosslinking sites that can support good environment stability of the gel against the transient change in pH or ionic strength under various physiological conditions at the delivery sites. Meanwhile, chemical crosslinking results in strong but tunable mechanical characteristics, or in other terms, the microstructure of the gels, to regulate the drug release profile more specifically. When CNF is composited with a secondary biopolymer, such as xylan or gelatin, chemical modification routes have been established to create chemically crosslinked CNF-based hydrogels via enzymatic or photochemical reactions (Laurén et al., 2017; Markstedt et al., 2017). Previously, we have extensively investigated binary systems of CNFs and water-soluble galactoglucomannan (GGM) as a nanocomposite hydrogel (Liu et al., 2016a,2016b; Markstedt et al., 2017; Xu et al., 2019a,2019b). GGM is the main type of hemicelluloses fractioned from softwood under a biomass-feed biorefinery (Xu et al., 2007). In plant cell wall structure, hemicelluloses firmly link together with cellulose fibers through a complex bonding network and this intrinsic affinity provides the cell wall a structural composite conferring both strength and flexibility. After being fractionated from biomasses, the high physical affinity between hemicellulose and cellulose surface is retained and this gives hemicelluloses an applicable niche as anchor polymers to engineer the surface of cellulose fibers (Xia et al., 2021; Trombino et al., 2019). To composite the hemicellulose with CNF in constructing hydrogel is in particular inspired by this biomimetic perspective and the crosslinking strategy has been exampled with upon UV via photopolymerization or upon enzymatic reaction, such as methacrylated GGM (Xu et al., 2019a,2019b) and tyramine-grafted GGM (Markstedt et al., 2017).

For an up-to-date hydrogel DDS, stimuli-responsiveness that is capable of on-demand delivery of the encapsulated drugs as a response to an external physical stimuli (often referring to a thermal, photo, or electrical signal input), is a strongly desired feature to integrate. This function enables real-time and in situ control over the hydrogel DDS to result enhanced therapeutic effects via encapsulated trigger release of goods (Chen et al., 2016; Wang et al., 2022a; Wang et al., 2022b; Yu et al., 2017). One strategy to create a redox-responsive hydrogel is to graft functional ligands containing thiol groups (-SH) in the derivation of natural polymer to make use of the reversible thiol-disulfide exchange reaction. This strategy is effective both towards achieving the chemical crosslinking upon UV-radiation and enabling the breaking down of the crosslinking bonds upon the redox stimuli delivered with either a reducing agent or a reducing electrical potential (Lee et al., 2019; Wang et al., 2016; Zhang et al., 2022; Zhao et al., 2019). Wang et al. (Wang et al., 2016) reported a method for constructing biodegradable hydrogels with specific properties using UV-triggered sulfhydryl-disulphide interchange reaction, providing precise spatiotemporal control over the structures and properties of disulfide crosslinked hydrogels. It is postulated that a thiol derivative of GGM can act as a surface-engineering biopolymer for the nanocellulose to viably bridge the dynamic responsiveness to the hydrogel via the sulfhydryl-disulphide interchange. We further hypothesize that this responsiveness is indicative for controlled delivery of biologics through the nanocomposite hydrogel of CNF and GGM. More relevantly, Laleh Maleki et al. (Maleki et al., 2015) have previously reported a one-pot synthesis of sulfhydryl-modified hemicellulose and developed the robust synthesis of subsequent various hemicellulose-based products through 'click' reactions. Inspired by this peer study, we have adapted their synthesis strategy to prepare the thiolated GGM (GGMSH) and aim to develop a photochemical crosslinked method to prepare disulfide-crosslinked dynamic reversible hydrogels with T-CNF for a controlled release of biologics, as illustrated in Scheme 1.

Bovine serum albumin (BSA) is proposed as a model protein to be encapsulated in the nanocomposite hydrogel of T-CNF and GGMSH. It is worth noting that BSA protein is composed of 585 amino acid residues containing 17 disulphide bridges, a free sulfhydryl group, and numerous disulfide bonds as well as free thiol groups that are hypothesized to take part in the reversible thiol-disulfide exchange reaction (Xia et al., 2021). The rheological properties, mechanical characteristics, chemical structure, and release profile of the hydrogel loaded with BSA were investigated systematically. In addition, the cytocompatibility of the nanocomposite hydrogel was evaluated in a 2D culture of normal human dermal fibroblasts (NHDF) for preliminary validating the as-proposed system as a bio-interfacing matrix.

2. Material and methods

2.1. Materials

Dimethyl sulfoxide anhydrous, 99.9%, sodium hydride, 60% dispersion in mineral oil, γ-thiobutyrolactone (TBL), ammonium chloride, 99.5%, 5,5′-dithiobis (2-nitrobenzoic acid) (Ellman's reagent), bovine serum albumin (BSA), 2-hydroxy-4′-(2-hydroxyethoxy)−2-methylpropiophenone (Irgacure 2959, 98%), rhodamine B, L-glutathione (GSH) and Coomassie (Bradford) Protein Assay Kit were all supplied by Sigma-Aldrich. GGM was obtained with hot water extraction (Xu et al., 2019a,2019b) and the chemical composition was characterized as shown in Table S1. According to a method reported earlier by Liu et al (Liu et al., 2014), the T-CNF dispersion was produced from softwood pulp by TEMPO/NaClO/NaBr oxidation followed by high-pressure homogenization. Material specifications of the as-synthesized T-CNF refer to a dry content matter of 1.8 wt% and a surface charge originated from carboxylic groups of 1.45 mmol/g.

2.2. Synthesis of GGMSH

GGMSH was synthesized by the ring opening of γ-thiobutyrolactone using the pendant hydroxyl groups of GGM as nucleophiles, according to a previous report by Laleh Maleki et al. (Maleki et al., 2015). Specifically, 20 mL of anhydrous DMSO was used to dissolve 0.33 g GGM in a beaker. Then, under a N_2 atmosphere, the above solution was added to a three-neck round bottom flask containing 0.024 g NaH equipped with a magnetic stirrer. After about 20 min, the GGM/DMSO solution was at once dropped and stirred continuously for 30 min to obtain a

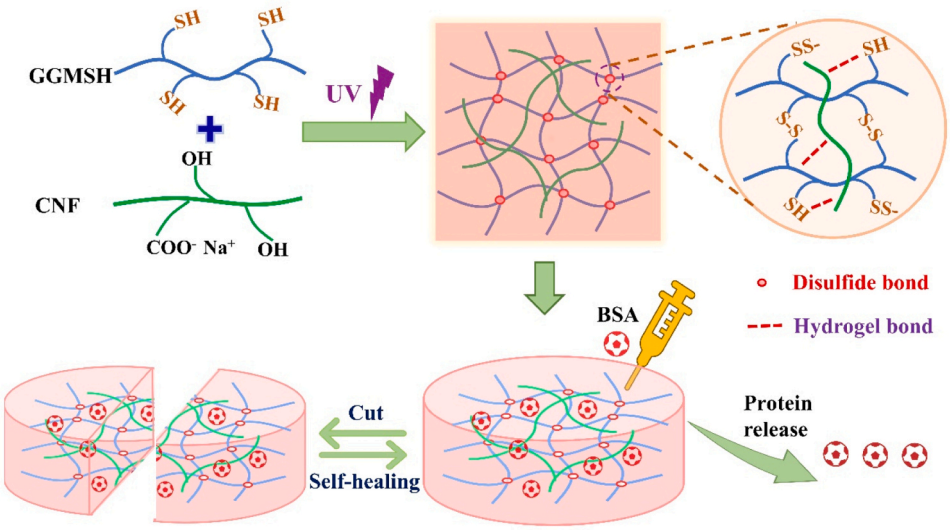

Scheme 1. The mechanism of fabricating hydrogels via a UV trigger thiol–disulfide crosslinked reaction.

homogeneous solution. Next, 65, 130, or 260 μL of TBL (0.75, 1.5, or 3 mmol) was added dropwise to the aforementioned three-neck round bottom flask and allowed the mixture to react at room temperature for 2 h. The reaction was quenched by adding 2 mL saturated NH_4Cl solution to the mixture. After further stirring for 10 min, the final mixture was precipitated into cold acetone, and a solid material was collected using centrifugation at 5000 rpm for 10 min. The solid material was repeatedly washed with ethanol for a second precipitation and centrifugation step. The solid material was then dissolved in deionized water, followed by dialyzing (500–1000 Da MWCO) against Milli-Q water until the conductivity of dialysis water reached similar values to that of deionized water. The purified material was freeze-dried to yield spongy GGMSH and its yield is around 70 −80%. The products obtained after the mercaptosylation of GGM with different dosages of TBL were denoted as GGMSHm, where m represents the amount of TBL used in the synthesis (0.75, 1.5, or 3 mmol).

The synthesized GGMSH was characterized by liquid-state ^{1}H NMR and liquid-state ^{13}C NMR. All the NMR experiments were measured with an NMR spectrometer (500.13 MHz for ^{1}H and 125.77 MHz for ^{13}C, AVANCE III, Bruker, USA) in D_2O at 298 K. The ^{1}H and quantitative ^{13}C experiments were recorded using a 5 mm Z-gradient BBO (Broadband Observe) cryoprobe. Based on quantitative ^{13}C NMR analysis, the degree of substitution (DS) of GGMSH was calculated by comparing the integral of the signals given by methylene carbon at δ 26.1 −26.7 ppm and the anomeric carbon at δ 97 −105 ppm.

2.3. Fabrication of GGMSH/T-CNF hydrogel

The UV crosslinkable hydrogel precursors were prepared by dissolving different contents of GGMSH3 (0, 1 vol%, 3 vol%, 6 vol%, and 9 vol%) and photoinitiator (0.5 wt% Irgacure 2959) into the T-CNF suspensions (1.5 vol%), and they were named C-GSH0, C-GSH1, C-GSH3, C-GSH6, and C-GSH9, respectively, as shown in Table 1. After vortex mixing for 5 min, different GGMSH/T-CNF hydrogel precursors were transferred to a transparent cylindrical mold with a diameter of 9 mm and a height of 4 mm, respectively. Then, the curing of hydrogel discs was carried out with a 365 nm UV-LED light source (85 mW/cm^2, bluepoint LED eco, Hönle Group) for 80 s

2.4. Characterization

2.4.1. Rheological behaviors

The rheological profiles of GGMSH/T-CNF hydrogel precursors were recorded by a Multi Drive rheometer (Anton Paar Physica MCR 702) using a plate-plate geometry (diameter: 25 mm) with a gap distance of 0.25 mm at 25 °C. Shear viscosity curves of hydrogel precursors were registered with a shear rate ranging from 0.1 to 1000 s^{-1}. To measure the strength of the hydrogel precursors, oscillatory strain sweeps ranging from 0.01% to 250% were performed at 1 Hz frequency to determine the linear viscoelastic region (LVR). A strain of 0.1% was found to be within the LVR of all tested hydrogel precursors. The dynamic strain step tests of the hydrogel precursors were performed by oscillating the sample at 0.1% strain for 80 s, followed by shearing at 80% strain for 60 s and then oscillating at 0.1% strain for 80 s at a constant frequency of 1 Hz. Photo-crosslinking kinetics of the hydrogel precursors were evaluated by registering the storage modulus (G′) with an oscillation mode under a constant strain and frequency of 0.1% and 1 Hz at a gap distance of 0.25 mm, respectively. The tested samples were irradiated with a 365 nm UV-LED light source (85 mW/cm^2, bluepoint LED eco, Hönle Group) starting at 30 s and stopped after irradiation at 110 s of the measurement. All measurements were tested in three replicates.

Table 1
Ink formulations with T-CNF and GGMSH.

Ink	GGMSH3 (vol%)	compositional ratio between T-CNF and GGMSH
C-GSH0	0	-
C-GSH1	1	3:2
C-GSH3	3	1:2
C-GSH6	6	1:4
C-GSH9	9	1:6

Note: The T-CNF content in all GGMSH/T-CNF inks are 1.5 vol%.
A hydrogel precursor composed of 6 vol% GGMSH3 and 1.5 vol% T-CNF was selected and loaded with different contents (0, 0.15, 0.3, or 0.45 vol%) of BSA to prepare BSA-containing hydrogel precursors, as shown in Table 2.

2.4.2. Mechanical properties

The compression measurement of formulated hydrogel disc (after UV irradiation 320 s) with a diameter of 9 mm and a height of 4 mm was carried out by the Anton Paar Physica MCR 702 rheometer under the compression mode. The compression speed was set with a constant rate of 0.01 mm/min. Young's modulus of the GGMSH/T-CNF/BSA hydrogel was calculated by extrapolation and linear fitting of the elastic region of stress-strain curve. Six hydrogel discs were prepared for each formulation.

2.4.3. Circular dichroism (CD) spectra

The circular dichroism (CD) spectra of different samples was performed with Chirascan spectrometer (Applied Photophysics Ltd) using a cuvette of path length 4 mm at 25 °C. The spectra were measured in the range 180–260 nm with a scan rate of 10 nm·min^{-1} and a response time of 2 s

2.4.4. Scanning electron microscopy (SEM)

Morphological features of the hydrogel structure were characterized by SEM-EDXA (EDXA, LEO Gemini 1530 with a Thermo Scientifc UltraDry Silicon Drift Detector, X-ray detector by Thermo Scientifc). The cryogels were fractured in liquid nitrogen, glued onto a sample stage, and sputtered with a thin layer of gold.

2.4.5. Swelling tests

The hydrogel discs were washed with Milli-Q water and then frozen by liquid N_2 prior to freeze-drying. When the freeze-dried discs were rehydrated with Milli-Q water, the gravimetrical water uptake was measured after the excess water on the surface was carefully removed with tissue paper. Then, the swelling ratio was calculated according to Eq. 1.

$$\text{Swelling ratio}(\text{g}/\text{g}) = \frac{W_{wet} - W_{dry}}{W_{dry}} \quad (1)$$

In addition, hydrogel discs without freeze-dried were also immersed in Milli-Q water. After carefully removing excess water from the surface with tissue paper, the weight and diameter changes of hydrogel were measured.

2.4.6. Self-healing performance

Two hydrogel discs (C-G-0.3%BSA, after UV irradiation 320 s) were prepared by the abovementioned method. The hydrogel was cut into two pieces, respectively. Half of the hydrogels were stained with rhodamine B. Two semicircles with different colors were placed on the petri dish, and the self-healing of the hydrogel was observed after UV irradiation at the time of 160 s.

2.4.7. Characterization of BSA release

Hydrogel degradation was monitored by tracking the release of the encapsulated BSA payload. The BSA loaded hydrogels were stored in glass vials that contained PBS solution only (5 mL) or L-glutathione in PBS solution (7.5 mM, 5 mL). The vials were masked with aluminium foil and incubated in an oven maintained at 37 ℃ with 100 rpm. At selected intervals, aliquots (30 μL) were taken from each vial and incubated with 1.5 mL Coomassie (Bradford) Protein Assay Kit for 10 min, followed by UV–vis spectrophotometry. Each sample was evaluated with at least three replicates. The analyzed samples were replenished with 30 μL and continued the release of BSA. The protein released at each time interval was quantified from the previously obtained linear calibration diagram.

2.4.8. Cell maintenance

Normal human dermal fibroblasts (NHDF) were purchased from PromoCell (C-12302, Germany). After recovering from cryopreservation, NHDF cells were maintained in complete culture medium (Dulbecco's Modified Eagle Medium, DMEM, GibcoTM, 41966029) supplemented with 10% heat-inactivated fetal bovine serum (Gibco®, 10270106) in an incubator (+37 °C, 5% CO_2). The medium was routinely changed once after 24 h incubation, and cells were passaged at sub-confluency.

2.4.9. Cytocompatibility

The cytotoxicity test was performed by incubating NHDF cells with GGMSH/T-CNF/BSA hydrogel matrices for a 10-day period. One day before the incubation, the hydrogel matrices with a diameter of 8.66 mm and thickness of 1.7 mm were portioned equally and placed separately in a 24-well plate. Each hydrogel matrix was photo-crosslinked by exposure to a UV light source (365 nm, a power of 85 mW/cm^2, duration for 80 s). Then the hydrogels were soaked in Dulbecco's Phosphate-Buffered saline (DPBS+, Gibco™ 14040091) at 37 °C to leach non-crosslinked components out. In 24 h, the matrices were washed twice with 1 mL fresh DPBS+ buffer prior to cell seeding.

Prior to seeding hydrogels, NHDF cell viability was assessed using haemocytometer (Bürker, 8100101). Cells were constantly maintained at viability of above 98% while passaging. One milliliter NHDF cell suspension with 5000 cells was seeded onto each hydrogel and cultured in incubator (Day 0). Both in vitro cytotoxicity test and imaging were performed at an incubation period of first, third, fifth and tenth day after cell seeding, coding term as Day 1, 3, 5, & 10.

In vitro cytocompatibility tests were performed using a CCK-8 kit (Dojindo Molecular Technologies, Inc, CK04–11) according to the supplier's manual. At each designated time point, the hydrogels were washed with DPBS+ . One milliliter of cell medium and 100 μL of CCK-8 reagent were added to each hydrogel-containing well. After 2.5 h of incubation, the assay solution was transferred into a new 96-well plate with a volume of 100 μL/well. The optical density (OD) was read at 450 nm using a microplate reader (Varioskan Flash, Thermo Scientific). To subtract the background, the same amount of cell medium and scaffolds for each formulation without cells was tested in the same way. The assay solution from the well with NHDF cells incubated using the same amount of cell medium in the absence of hydrogel was tested in the same way as a reference. The absorbance signal from 100 μL cell medium was subtracted as background for the NHDF cells incubated in the absence of hydrogel.

To assess the cell viability, confocal images were taken after culturing with hydrogels with staining NHDF cells using Live/Dead Cell Staining Kit II (PK-CA707–30002, PromoKine). Calcein AM (a cell-permeable green fluorescent dye) and EthD-III (a cell-impermeable red fluorescent dyes) were used to differentiate dead and living cells. One millimeter staining solution containing 0.25 μM Calcein AM, and 0.5 μM EthD-III dissolved in PBS was added into each well after washing the incubated cells with DPBS+. After 40 min incubation, cells were brought for confocal image capture with the 10x objective equipped with an ORCA camera. Green fluorescent signal from Calcein AM was obtained by LED illumination at 488 nm. Red fluorescent signal from PI was obtained by LED illumination at 561 nm. Images were further processed with SlideBook 6 Reader and FIJI ImageJ software. Imaging of NHDF cells cultured in the absence of hydrogels in the 24-well plate was conducted as a live control.

3. Results and discussion

3.1. Synthesis and characterization of GGMSH

The synthesis the thiol derivative of GGMSH was carried out according to the previous method by Laleh Maleki et al (Maleki et al., 2015). First, NaH was used for deprotonation of polyhydroxylated GGM. Then, γ-thiobutyrolactone was ring-opened by nucleophilic attack of the activated pendant hydroxyl group on the GGM backbone. The ring opening of TBL results in covalent grafting of mercaptan groups to hydroxyl groups of GGM, as confirmed by NMR spectroscopy. Fig. 1a and b display the chemical shifts caused by methylene protons and carbon atoms in ^{1}H and ^{13}C NMR spectra of all GGMSH samples. The chemical shift of 2.6 ppm corresponds to the methylene proton adjacent to the mercaptan groups (C12). The peak at about 1.89 ppm originates from the proton response of C11 methylene. The proton response of the methylene group adjacent to the carbonyl group is possibly overlapped with the CH_3 of the acetyl group in GGM. In the quantitative ^{13}C NMR spectra of GGMSH3, three additional peaks of C12, C11, and C10 at 26, 31, and 35 ppm were observed after TBL ring-opening (Fig. 1b). Moreover, the corresponding peak value of lactone carbonyl group after TBL

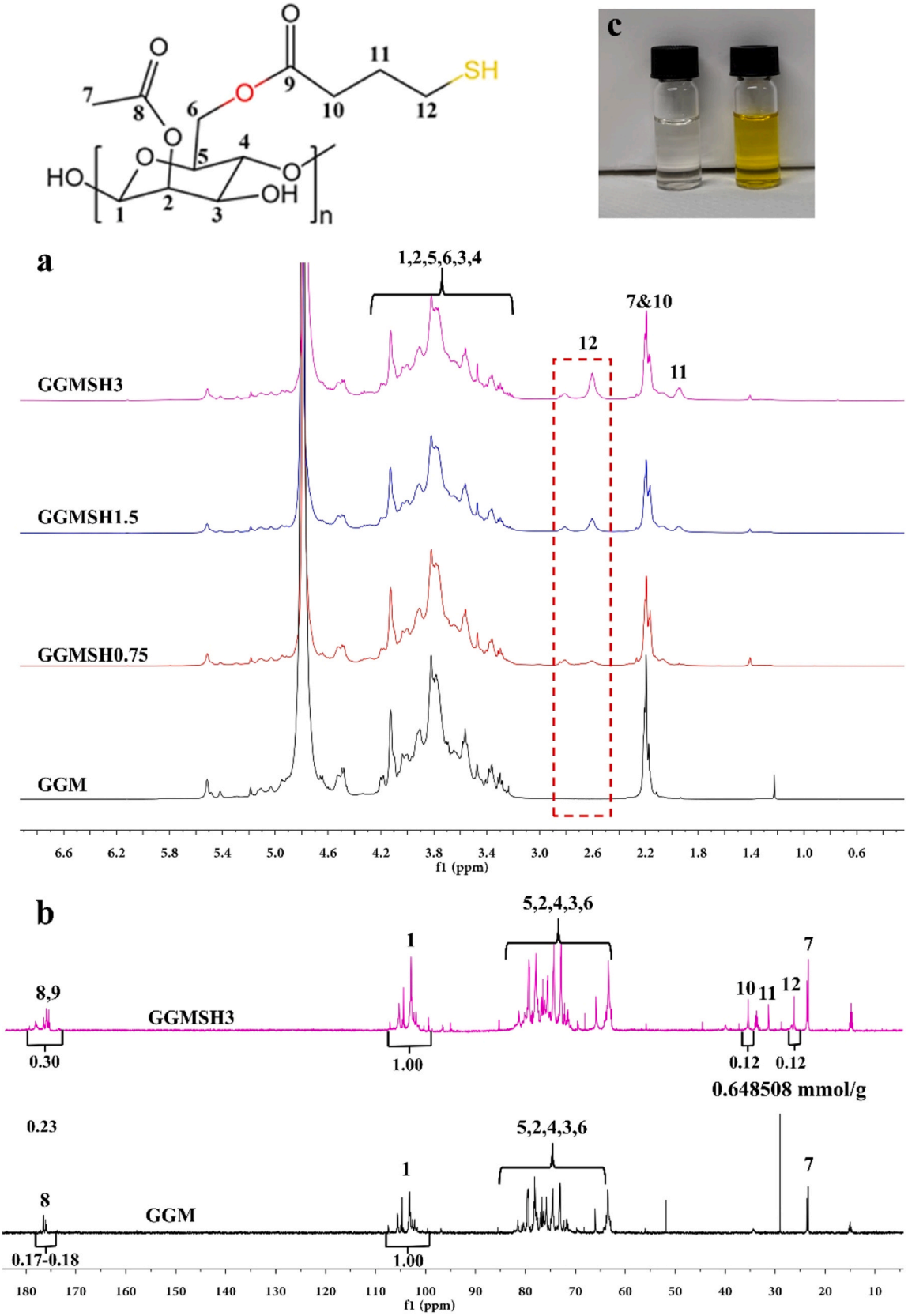

Fig. 1. (a) ^{1}H NMR spectra of GGM and GGMSH, (b) quantitative ^{13}C NMR spectra of GGM and GGMSH3. (c) Solution of GGMSH3 in sodium phosphate buffer (left), instantly turning yellow upon the addition of Ellman's reagent (right).

ring opening appeared at 177 ppm. According to the integral comparison based on the anomeric carbon (δ 97 −105 ppm), the degree of thiol substitution (DS_{SH}) for each product (GGMSH0.75, GGMSH1.5, and GGMSH3) could be obtained from the featured peaks of the methylene carbon (δ 26.1 −26.7 ppm), methylene carbon (δ 31.2 −32.9 ppm), and the lactone carbonyl group (δ 176.5–179.3 ppm), as summarized in Table 3.

Ellman's reagent analysis was further used to confirm the successful ring opening of TBL and the presence of sulfhydryl groups in the modified GGM chain. First, after mixing Ellman's reagent with GGMSH solution, the nitromercaptobenzoate anion released into the reaction mixture immediately formed a strong yellow, thus confirming the existence of sulfhydryl group in the modified GGM, as shown in Fig. 1c. Next, the mercaptan content per 100 mg modified GGM was calculated by using the molar absorbance of Ellman's reagent at 412 nm.

The DS_{SH} of synthesized GGMSH's SH was further quantified through elemental analysis, as detailed in the supplementary materials (Table S2). By comparing the results obtained from Ellman's reagent, elemental analysis with the DS_{SH} calculated from ^{13}C NMR spectra of the modified GGM, a rough estimation of the number of thiol groups per modified GGM chain was computed, as shown in Table 3. Meanwhile, the average number molar mass (M_n) of the GGMSH measured by HPSEC increased from 5.94 kDa of GGM to 15.4 kDa of GGMSH3 due to the increased DS value. The GGMSH3 with the highest DS_{SH} (0.65 mmol/g) as achieved in the optimization of GGMSH synthesis was chosen to fabricate hydrogels with T-CNF. As a result, a decent crosslinking density of disulphide bridges are expected to reach to guarantee the designated mechanical performance as well as the encapsulation of the protein inside the hydrogel.

3.2. Physical and chemical properties of GGMSH/T-CNF hydrogel

Firstly, the rheological properties of the GGMSH/T-CNF hydrogel precursors were promptly evaluated. Typical shear-thinning profiles were observed for all the hydrogel precursors, as shown in Fig. 2a. The viscosity of hydrogel was decreased by increasing shear rate. The addition of GGMSH did not alter the shear-thinning behavior, indicating that the series of GGMSH/T-CNF hydrogel precursors are suitable for injectable molding. The shear-thinning behavior can be attributed to the shear fracture of the dynamic hydrogel network. In addition, the viscosity increased with the increase of the GGMSH content. At the same time, compared with the pristine CNF hydrogel, the addition of GGMSH increased the zero-shear viscosity of GGMSH/T-CNF hydrogel precursor. As displayed in Fig. 2b, viscoelastic properties of GGMSH/T-CNF hydrogel precursor were analyzed by amplitude sweep, and changes of storage modulus (G′) and loss modulus (G") relative to shear stress were measured. The flow stresses (shear stress at the intersection of G′ and G") of all hydrogels were higher than 10 Pa. The G′ and flow stress of the GGMSH/T-CNF hydrogel precursors increased with the increase of GGMSH content. These results might be due to the strong hydrogen bonds between thiol groups in GGMSH and the T-CNF, which makes GGMSH physically trapped in the T-CNF hydrogel network.

The photo-crosslinking kinetics of the GGMSH/T-CNF hydrogel precursors were also measured using photo-rheology, as shown in Fig. 2c. The storage modulus of hydrogel precursors was recorded for 80 s while UV was turned on at 30 s. Compared with pristine T-CNF hydrogel, all GGMSH/T-CNF hydrogel precursors crosslinked after UV irradiation with a slow kinetic, as indicated by the slow gradual increase of G′. The addition of GGMSH resulted in an increase in G′, and the G′ value increased significantly with the increase of GGMSH content. The G′ kept static once the UV radiation was turned off, corresponding to a halt of crosslinking process. These findings suggested that mercaptan crosslinking formed disulfide bond crosslinking points among GGMSH, which is well triggered by UV radiation. The process of generating dynamic crosslinked hydrogels by UV-triggered thiol–disulfide exchange reaction is depicted in Scheme 1. In the initial stage, the photoinitiator (IR2959) generates carbon free radicals under UV irradiation, and then extracts the hydrogen protons of the sulfhydryl group in GGMSH to generate sulfhydryl free radicals. The disulfides are formed between GGMSH molecular chains and interspersed with T-CNF to form a crosslinked network.

Table 2
Ink formulations with T-CNF, GGMSH and BSA.

Ink	GGMSH3 (vol%)	BSA (vol%)
C-G-0 BSA	6	0
C-G-0.15%BSA	6	0.15
C-G-0.3%BSA	6	0.3
C-G-0.45%BSA	6	0.45

Note: The T-CNF content in all GGMSH/T-CNF/BSA inks are 1.5 vol%.

Table 3
DS of the thiol groups and the average molar mass distribution of the GGM and GGMSH materials.

Code	DS of thiol groups	Thiol groups[a] (mmol/g)	Thiol groups[b] (mmol/g)	Thiol groups[c] (mmol/g)	M_n/ kDa[d]
GGM	0	0	0	0	5.94
GGMSH0.75	0.05	0.27	0.07	0.06	11.89
GGMSH1.5	0.07	0.38	0.12	0.13	15.21
GGMSH3	0.12	0.65	0.31	0.66	15.40

[a] Calculated results based on quantitative ^{13}C NMR. [b] Results calculated using molar absorptivity of Ellman's reagent at 412 nm. [c] Results calculated using Elemental analysis. [d] M_n determined from HPSEC.

The role of BSA on the viscosity, viscoelastic behavior and photo-crosslinking kinetics of GGMSH/T-CNF/BSA hydrogel was further systematically studied. The results showed that the viscosity and flow stress of GGMSH/T-CNF/BSA hydrogel precursors increased with an increase in BSA content, as illustrated in Figure S1. Similar to GGMSH/T-CNF, all GGMSH/T-CNF/BSA hydrogel precursors underwent gradual crosslinking upon UV irradiation (Fig. 2d). In addition, the G′ of GGMSH/T-CNF/BSA hydrogel precursor was observed to increase with an increase in BSA content. The unique nanostructure of BSA and the presence of functional groups such as disulfide bond and sulfhydryl group within its protein structure might have played a role in the physical and chemical crosslinking of GGMSH in the hydrogel system, which could lead to the increase in G′.

The mechanical strength of hydrogels after gelation is crucial for their performance in biological environments. In this study, we evaluated the mechanical strength of GGMSH/T-CNF/BSA hydrogel discs through compressive testing and found that the addition of BSA improved the hydrogel's mechanical properties (Fig. 2e) Specifically, the hydrogel containing 0.3% BSA (C-G-0.3%BSA) showed a significant increase (up to 35 kPa) in compressive Young's modulus. This increase in mechanical strength can be attributed to the formation of a dense crosslinking network, as evidenced by rheological analysis. It is postulated that the unique nanostructure of BSA and the presence of functional groups such as disulfide bond and sulfhydryl group in the protein structure of BSA may have contributed to the physical and chemical crosslinking with GGMSH in the hydrogel system.

To further verify the anticipation, circular dichroism spectroscopy was used to confirm the expected cross-linking reaction in the GGMSH/T-CNF/BSA hydrogel system, with the CD spectra scanned between 180 and 260 nm. Fig. 2f shows the CD spectra of BSA without or with different GGMSH concentrations. BSA exhibited a positive ellipticity at about 198 nm and a negative ellipticity at 238 nm, which represent typical α-helix structure of the protein (Pang et al., 2017; Wang et al., 2017). Binding of GGMSH to BSA resulted in a decrease in the negative ellipticity of CD at all wavelengths in the far ultraviolet, indicating a change in the protein secondary structure (a decrease in the α-helix content of BSA) (Wang et al., 2017; Xia et al., 2021). As the secondary

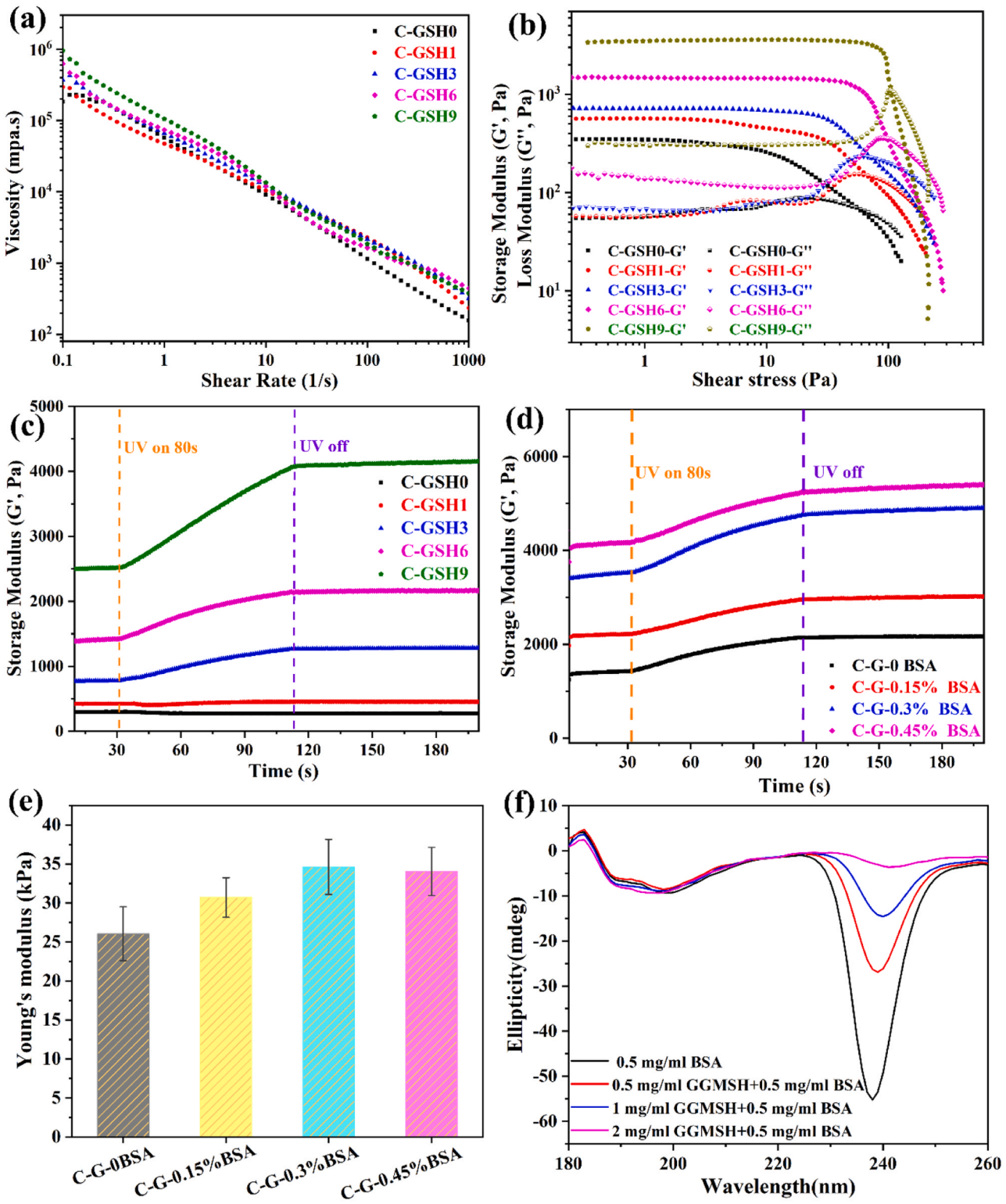

Fig. 2. Viscosity (a), viscoelastic behavior (b), and photo rheology profiles (c) of the hydrogel precursors (C-GSH0, C-GSH1, C-GSH3, C-GSH6, and C-GSH9); Photo rheology profiles of the hydrogel precursors with different content BSA (d), and (e) compressive Young's moduli of the cast hydrogel disc with different contents of BSA (C-G-0 BSA, C-G-0.15%BSA, C-G-0.3%BSA, and C-G-0.45%BSA); (f) CD spectra of BSA (0.5 mg/mL) reacted with different concentrations of GGMSH.

structure content of protein is closely related to its biological activity, these changes observed in the secondary structure of BSA may lead to the loss of biological activity of BSA. This may be caused by the inter- and intramolecular disulfide bridging of GGMSH with the amino acid residues of the BSA polypeptide chain, meanwhile reducing the hydrogen bonds within the protein (Paul et al., 2017; Raja et al., 2015; Wang et al., 2017; Yue et al., 2014).

3.3. Self-healing ability

The reversible nature of the chemical crosslinking via thiol-disulfide exchange reaction allows the GGMSH/T-CNF/BSA hydrogels to exhibit

fast self-healing properties (Mredha et al., 2020; Yoon et al., 2012; Yu et al., 2017). Fig. 3 demonstrated the self-healing capability of the hydrogel, via a cut-contact-UV irradiation experiment. Initially, two coin-shaped C-G-0.3%BSAhydrogels (GGMSH/T-CNF/BSA hydrogels containing 0.3% BSA) were prepared, with one sample stained with Rhodamine B to facilitate observation. The hydrogel sample was cut in half, and the two different colored halves were attached to each other at room temperature. The disulfide cross-linking network in the recombinant hydrogel system facilitated the successful recovery of hydrogel sample into one piece after 160 s UV irradiation. Additionally, the self-healed hydrogel samples were able to remain intact without any separation when soaked in water after recovery, as shown in Fig. 3a and Video S1. Based on these results, it was confirmed that C-G-0.3%BSA exhibits effective self-healing property during the cut-contact-UV process. The present results are consistent with the phenomena that were reported elsewhere (Lee et al., 2019; Zhang et al., 2022; Zhao et al., 2019). The rheological properties of hydrogel system were further investigated to understand its self-healing capabilities. The modulus-strain relationship at a constant frequency of 1 rad/s was monitored to identify the linear viscoelastic region and the crossover strain of gel-sol transition. Both G′ and G" remained constant in the strain range of about 0.1%, as displayed in Fig. 3b. As the strain increased beyond this range, both G′ and G" declined significantly, and reached a crossover at around 10% of strain variables. Once the critical strain limit was surpassed, the G" surpassed G′, indicating complete destruction of hydrogel. Initially, the hydrogel exhibited solid-like viscoelastic behavior, with G′ being higher than G". The self-healing properties of C-G-0.3%BSA hydrogel was further tested through continuous step strain sweeps at a shear strain change between (0.1% or 80%), as displayed in Fig. 3c. The hydrogel initially behaved as solid-like viscoelastic gel at the strain of 0.1% (G′ > G"). However, the hydrogel underwent a transformation into a liquid-like viscoelastic state (G′ < G"),

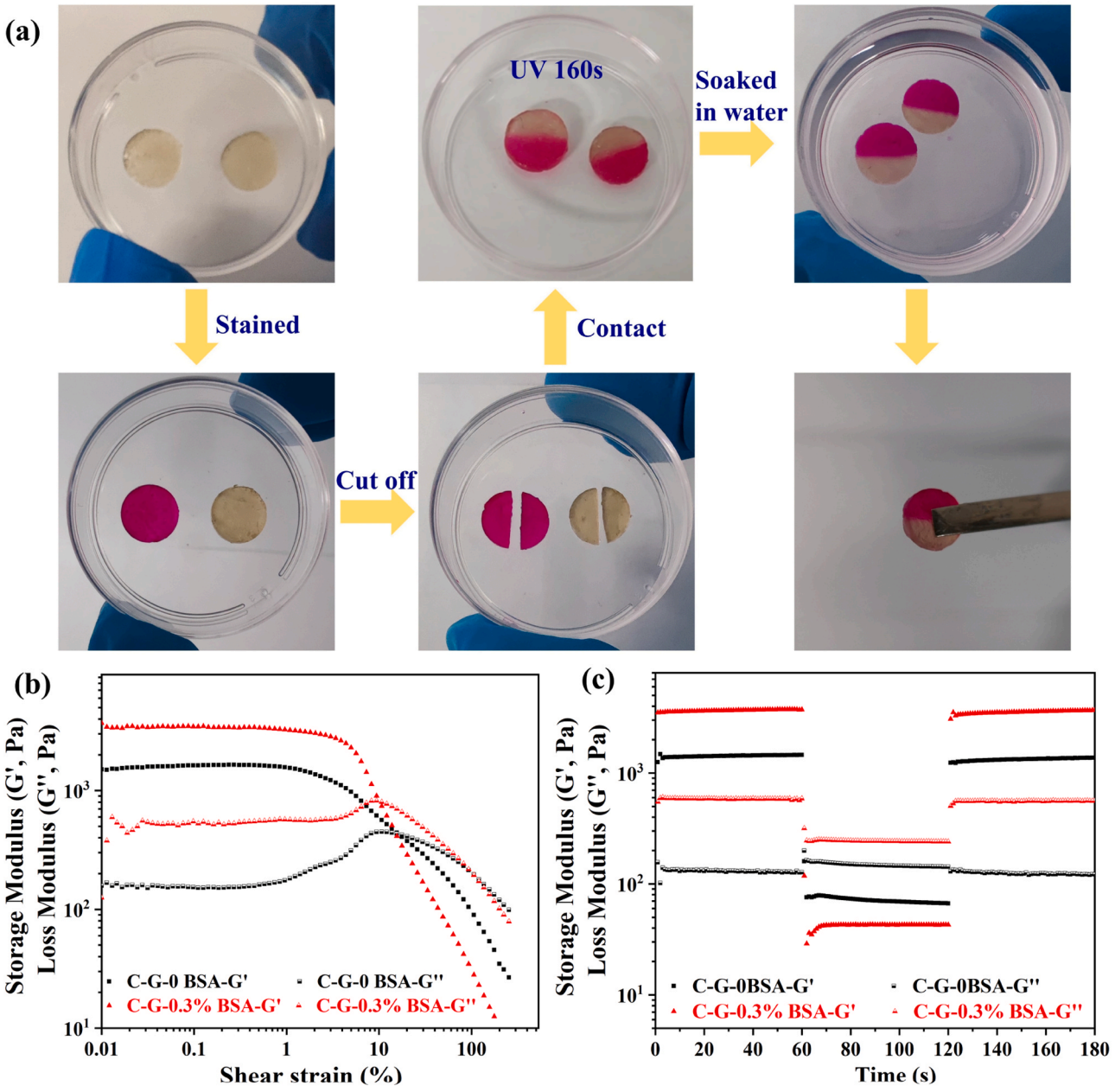

Fig. 3. (a) Demonstration of self-healing ability of C-G-0.3%BSA hydrogels. (b) Dependence of moduli of C-G-0BSA and C-G-0.3% BSA hydrogels on strain amplitude sweep (γ = 0.01 −250%) at a fixed frequency of 1 rad/s. (c) Step-strain test of C-G-0BSA and C-G-0.3% BSA hydrogels at a fixed frequency of 1 rad/s (0.1% or 80% of strain).

as the hydrogel network collapsed (Shi et al., 2017). Upon returning to the shear strain from 80% to 0.1%, hydrogel immediately reverted to their initial gel state keeping as similar G′ and G" levels as before under high shear, indicating its remarkable self-healing capacity.

Supplementary material related to this article can be found online at doi:10.1016/j.indcrop.2023.117615.

3.4. Swelling, rehydration, and BSA release properties of hydrogel

Swelling performance and the rehydration behavior of hydrogels are essential factors to consider for its biomedical applications. Typically, the swelling capacity is usually linked to the hydrophilicity and density of hydrogels. Rehydration capacity directly reflects a hydration ability and stability, which is also related to the mechanical stiffness and structural properties (Xu et al., 2019a,2019b; Zhang et al., 2020). In our case, freeze-dried hydrogels (C-G-0BSA and C-G-0.3%BSA hydrogels) were soaked in Milli-Q water, and their swelling behavior was recorded over time (Fig. 4a). The rehydration kinetics of both cryogels were similar, showing rapid rehydration within 1 min and reached equilibrium in 3–6 h. The GGMSH/T-CNF (C-G-0BSA) cryogels made of 1.5% T-CNF and 6% GGMSH could absorb water up to around 15 times its own dry weight. In the case of the addition of 0.3% BSA (C-G-0.3%BSA), the water uptake of GGMSH/T-CNF/BSA cryogel increased to 20 times its own dry weight. The rehydration behavior of GGMSH/T-CNF is attributed to the strong hydrogen bond between T-CNF and GGMSH fibers. The introduction of a small amount of BSA enhanced the swelling property and water absorption capacity of the cryogel, likely due to BSA's hydrophobic characteristics and electrostatic repulsion between BSA and T-CNF under pH= 7 (Esfahan et al., 2020; Solin et al., 2020).

The swelling behavior and rehydration behavior of pristine hydrogels were also investigated. The weight and diameter of GGMSH/T-CNF (C-G-0BSA) and GGMSH/T-CNF/BSA (C-G-0.3%BSA) hydrogels reached equilibrium within 3–6 h. It is also found when BSA is introduced, hydrogel demonstrated a higher rehydration ratio and swelling tendency. Besides evaluating the hydrogels' swelling performance and rehydration behavior, the compressive mechanical properties of C-G-0 BSA and C-G-0.3%BSA hydrogels were tested after being immersed in DPBS+ for 6 h before and after UV irradiation. The Young's modulus of hydrogels after UV irradiation is higher than that of hydrogels without UV irradiation (Fig. 4b), which is consistent with the result obtained by photo-crosslinking rheology. Moreover, the mechanical property of hydrogels in DPBS+ for 6 h was obviously lower than that of unsoaked hydrogels. In addition, the cross-section morphology of hydrogel was characterized. It was found that the section morphology did not change significantly after adding BSA, demonstrating microscopic morphology of T-CNF (Fig. 4c and Figure S2). In comparison with other reported T-CNF/hemicellulose hydrogels (Liu et al., 2016a,2016b; Xu et al., 2019a, 2019b), such as T-CNF/GGM, T-CNF/Xylan or T-CNF/GGMMA hydrogel, GGMSH/T-CNF hydrogel demonstrated an even wider-spectrum of tuneable mechanical strength.

Next, the potential use of glutathione to trigger the release of BSA in hydrogels by reducing disulfide bridges that maintain the network structure was evaluated. The BSA release was monitored for 48 h in the response to glutathione. It was found 70% of the protein was released from the C-G-0.3%BSA hydrogel after 6 h incubation at physiological temperature (Fig. 4f), and there was a slightly increase in hydrogel degradation. When the hydrogel was incubated only in PBS solution, nearly 80% of the BSA was released from the C-G-0.3%BSA hydrogel after 6 h incubation at physiological temperature, and then it tended to reach equilibrium and was no longer released. It seemed that the swollen response of GGMSH/T-CNF/BSA hydrogel greatly altered the mesh size of the hydrogel and the non-covalently bonded BSA was immediately released as the hydrogels swelled in PBS buffer.

3.5. Cytocompatibility

T-CNF hydrogels with porous three-dimensional (3D) network serve as an enticing platform matrix in therapeutic delivery. As illustrated

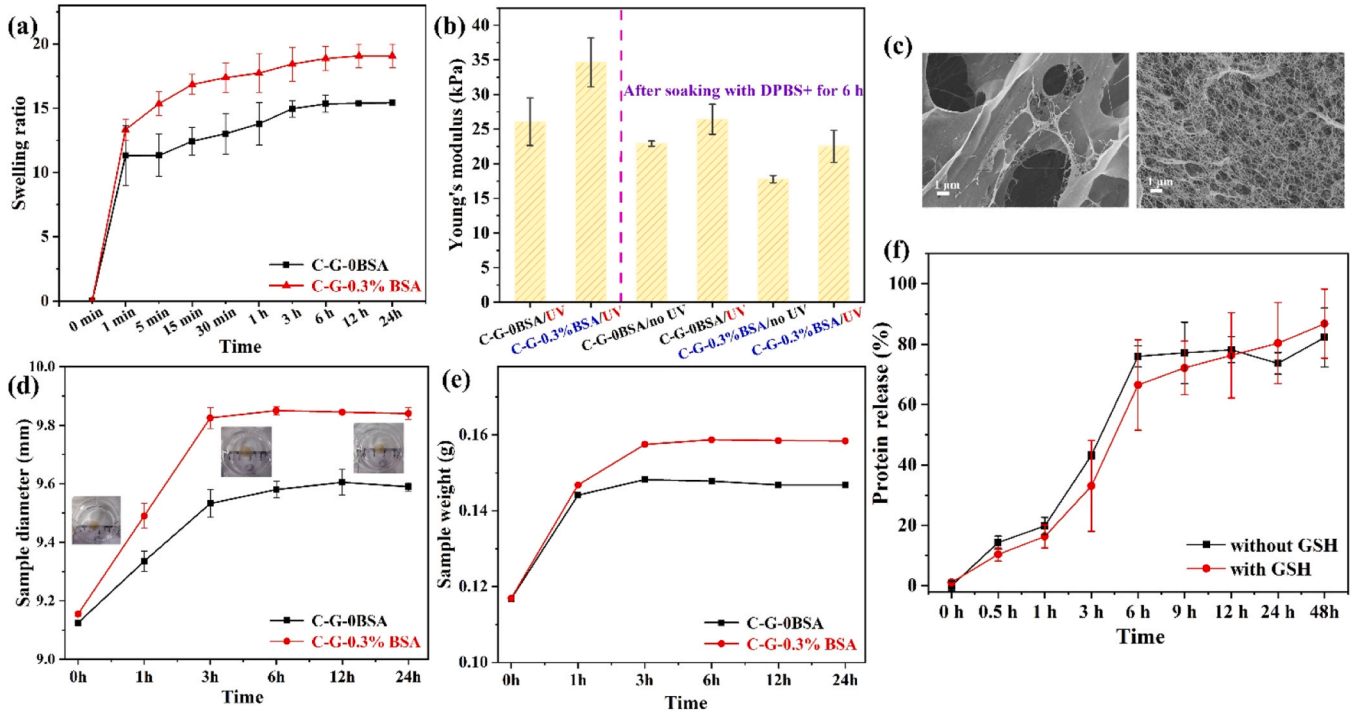

Fig. 4. (a) Rehydration behavior of the freeze-dried cryogels against time scale. (b) Compressive Young's modulus of the cast disc hydrogel without BSA and with 0.3% BSA after immersion in DPBS+ for 6 h before and after UV irradiation. (c) SEM images of casting disc cryogels without BSA and with 0.3% BSA cross-section. (d) Diameter and (e) mass change of nonfreeze-dried hydrogel soaked in Milli-Q water with time. (f) The release of BSA from C-G-0.3%BSA hydrogel in response to incubation in 7.5 M glutathione and in response to incubation in PBS solution only.

above, the incorporation of GGMSH renders GGMSH/T-CNF hydrogel composites possessing a tunable wide-spectrum mechanical property. Wherever GGMSH/T-CNF hydrogel is in subjected to possible biomedical applications, cytocompatibility of GGMSH/T-CNF hydrogels is the perquisite to be verified. In the sense, T-CNF hydrogels are usually proven to be cytocompatible with multiple cell lines, such as fibroblast and cancer cells (Rosendahl et al., 2021; Xu et al., 2018). In this section, both GGMSH/T-CNF composite hydrogels matrices and GGMSH/T-CNF/BSA (containing 0.15%, 0.3%, and 0.45% BSA) matrices in the case of studying model protein BSA release were tested for validating their non-cytotoxicity.

The cytotoxicity and cell proliferation results are shown in Fig. 5a. It was observed the optical absorbance (OD) values increased with growing cell incubation days for all the tested systems, which reveals an extended cell proliferation for all the systems. The OD values obtained from NHDF cells incubated with GGMSH/T-CNF/ BSA hydrogels are smaller on Day-1, Day-3, and Day-5, compared with those values in the absence of hydrogels. However, the OD values at Day 10 for NHDF cells reached the same magnitude on Day-10. In this sense, the presence of GGMSH/T-CNF hydrogel supports NHDF cell proliferation in a bit longer period with a proven non-toxicity to NHDF cells compared with 2D control. The suppression of cell proliferation may be due to the leaching of free radicals. It is reported that free radicals may create oxidative stress and are subsequently associated with cell damage (Calabrese et al., 2008; Rosendahl et al., 2021). The free radicals might be generated due to the dynamic exchange of covalent disulphide between free thiol groups in the hydrogel system (Wang et al., 2016). The live/dead staining assay was further performed on incubated NHDF cells at the presence and absence of GGMSH/T-CNF/BSA hydrogels. Cells are rarely dead (presenting a red signal) as revealed in the confocal images with staining the cells with live and dead assay (Fig. 5b and Figure S3), which supported the non-cytotoxicity of the hydrogels.

4. Conclusions

In summary, we demonstrated a dynamic reversible hydrogel with non-toxic and profound self-healing properties via synergetic effect between a formation of UV-triggered dynamic thiol-disulfide bond and the strong hydrogen bonds in GGMSH/T-CNF hydrogel. The resulting GGMSH/T-CNF hydrogel demonstrated a wide spectrum of tunable mechanical strength. Furthermore, the integration of BSA into the GGMSH/T-CNF hydrogel endowed a robust mechanical performance, while the hydrogel still maintained good cytocompatibility. Owing to the swelling response of GGMSH/T-CNF/BSA, an immediate release profile of BSA is registered in the current design of carrier system. Our study has established reference value to further develop the nanocomposite hydrogel of GGMSH/T-CNF as a delivery vector for controlled release of therapeutics in the field of biomedical research.

CRediT authorship contribution statement

Bi Hongjie: Methodology, Investigation, Visualization, Validation, Writing – original draft preparation. **Zhang Xue**: Methodology, Investigation, Validation, Writing – original draft preparation. **Wang Qingbo**: Methodology. **Yong Qiwen**: Methodology. **Xu Wenyang**: Methodology. **Xu Min**: Funding acquisition. **Xu Chunlin**: Resources, Funding acquisition. **Wang Xiaoju**: Conceptualization, Supervision, Funding acquisition, Writing – original draft preparation, Writing – review & editing.

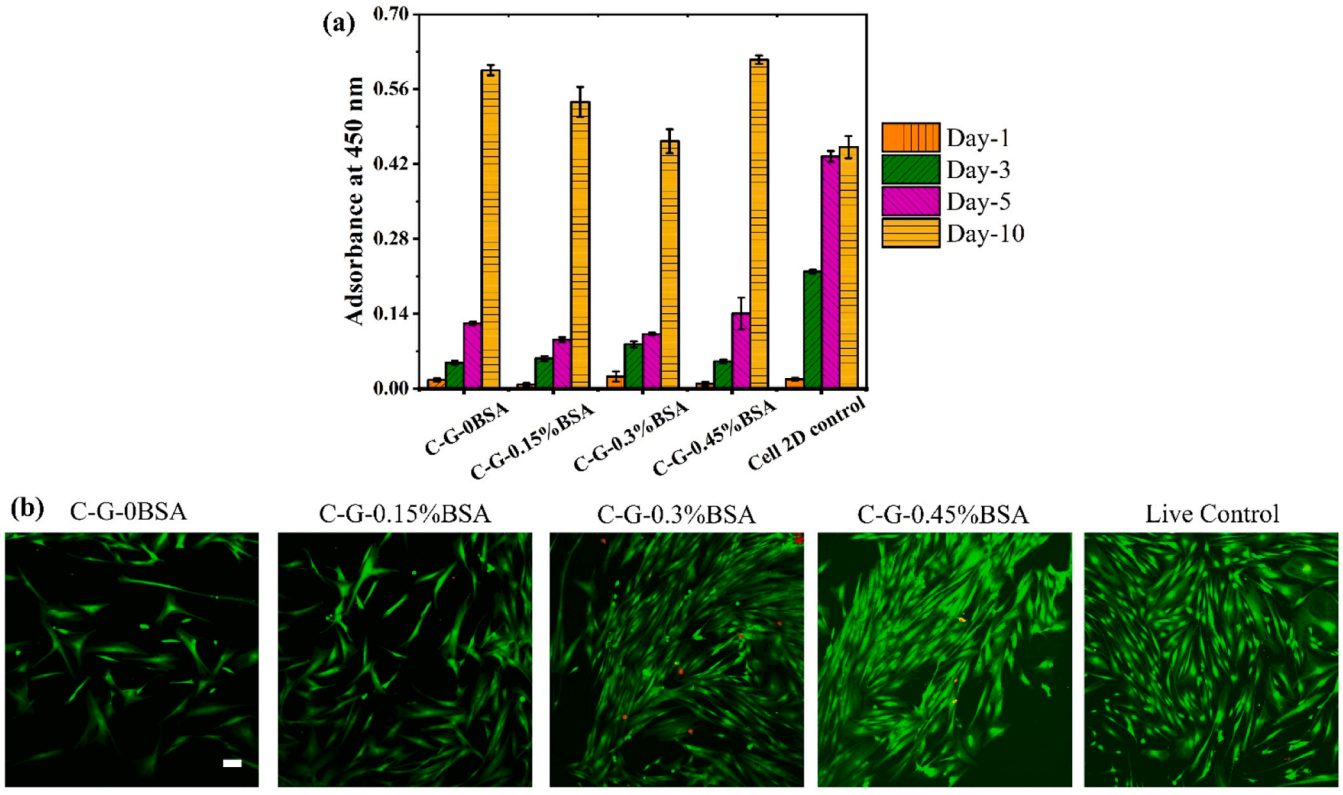

Fig. 5. (a) Optical absorbance values of NHDF cells obtained by CCK8 assay at Day-1, day-3, day-5 and Day-10. Error bar represents the standard deviation of the mean. (The experiment repetition number N = 7–10). (b) Confocal images of NHDF cells at a 10-day incubation with GGMSH/T-CNF matrices and 2D control obtained after live/dead staining. C=T-CNF, G=GGMSH, the number in front of BSA represents the concentration of stock BSA solution in percentage used to mix with the T-G hydrogel. The green signals reflect cells that are live, while the dead signal indicates the presence of dead cells. All the images share the same scale bar, which is 100 μm.

Declaration of Competing Interest

The authors declare that they have no known competing financial interests or personal relationships that could have appeared to influence the work reported in this paper.

Data availability

Data will be made available on request.

Acknowledgements

Dr. Hongjie Bi would like to acknowledge the financial support from the China Scholarship Council (Student ID 202006600009 for H. Bi) to her research visit at Åbo Akademi University (ÅAU), Finland. X. Zhang, W. Xu, and X. Wang would like to thank Academy of Finland (333158) as well as Jane and Aatos Erkko Foundation for their funds to the conducted research at ÅAU. Q. Wang and C. Xu would like to acknowledge the Finnish Ministry of Education and Culture funded international pilot project "Finland-China Food and Health Network" and the European Regional Development Fund (ERDF) for the project “AMBioPharma” (Centre for Additive Manufacturing for Life Science and Pharmaceutical Industry, project code A77805) on supporting this project.

Appendix A. Supporting information

Supplementary data associated with this article can be found in the online version at doi:10.1016/j.indcrop.2023.117615.

References

Auvinen, V., Laurén, P., Shen, B., Isokuortti, J., Durandin, N., Lajunen, T., Linko, V., Laaksonen, T., 2022. Nanoparticle release from anionic nanocellulose hydrogel matrix. Cellulose 29 (18), 9707–9717.
Basti, A.T.K., Jonoobi, M., Sepahvand, S., Ashori, A., Siracusa, V., Rabie, D., Mekonnen, T.H., Naeijian, F., 2022. Employing cellulose nanofiber-based hydrogels for burn dressing. Polymers 14 (6), 1207.
Calabrese, V., Bates, T.E., Mancuso, C., Cornelius, C., Ventimiglia, B., Cambria, M.T., Di Renzo, L., De Lorenzo, A., Dinkova Kostova, A.T., 2008. Curcumin and the cellular stress response in free radical-related diseases. Mol. Nutr. Food Res. 52 (9), 1062–1073.
Chen, C., Zheng, P., Cao, Z., Ma, Y., Li, J., Qian, H., Tao, W., Yang, X., 2016. PEGylated hyperbranched polyphosphoester based nanocarriers for redox-responsive delivery of doxorubicin. Biomater. Sci. 4 (3), 412–417.
Chinga-Carrasco, G., Syverud, K., 2014. Pretreatment-dependent surface chemistry of wood nanocellulose for pH-sensitive hydrogels. J. Biomater. Appl. 29 (3), 423–432.
Deng, W., Tang, Y., Mao, J., Zhou, Y., Chen, T., Zhu, X., 2021. Cellulose nanofibril as a crosslinker to reinforce the sodium alginate/chitosan hydrogels. Int. J. Biol. Macromol. 189, 890–899.
Esfahan, Z.M., Izhar, S., Halim, M., 2020. Synthesis and swelling kinetic study of BSA-based hydrogel composite by subcritical water technology. J. Environ. Treat. Tech. 8 (2), 756–761.
Klemm, D., Kramer, F., Moritz, S., Lindström, T., Ankerfors, M., Gray, D., Dorris, A., 2011. Nanocelluloses: a new family of nature-based materials. Angew. Chem. Int. Ed. 50 (24), 5438–5466.
Laurén, P., Somersalo, P., Pitkänen, I., Lou, Y., Urtti, A., Partanen, J., Seppälä, J., Madetoja, M., Laaksonen, T., Mäkitie, A., 2017. Nanofibrillar cellulose-alginate hydrogel coated surgical sutures as cell-carrier systems. PLoS One 12 (8), e183487.
Lee, S.H., Shin, S.R., Lee, D.S., 2019. Self-healing of cross-linked PU via dual-dynamic covalent bonds of a Schiff base from cystine and vanillin. Mater. Des. 172, 107774.
Liu, J., Korpinen, R., Mikkonen, K.S., Willför, S., Xu, C., 2014. Nanofibrillated cellulose originated from birch sawdust after sequential extractions: a promising polymeric material from waste to films. Cellulose 21 (4), 2587–2598.
Liu, J., Cheng, F., Grénman, H., Spoljaric, S., Seppälä, J., Eriksson, J.E., Willför, S., Xu, C., 2016a. Development of nanocellulose scaffolds with tunable structures to support 3D cell culture. Carbohydr. Polym. 148, 259–271.
Liu, J., Chinga-Carrasco, G., Cheng, F., Xu, W., Willför, S., Syverud, K., Xu, C., 2016b. Hemicellulose-reinforced nanocellulose hydrogels for wound healing application. Cellulose 23, 3129–3143.
Maleki, L., Edlund, U., Albertsson, A., 2015. Thiolated hemicellulose as a versatile platform for one-pot click-type hydrogel synthesis. Biomacromolecules 16 (2), 667–674.
Markstedt, K., Mantas, A., Tournier, I., Martínez Ávila, H., Hagg, D., Gatenholm, P., 2015. 3D bioprinting human chondrocytes with nanocellulose–alginate bioink for cartilage tissue engineering applications. Biomacromolecules 16 (5), 1489–1496.
Markstedt, K., Escalante, A., Toriz, G., Gatenholm, P., 2017. Biomimetic inks based on cellulose nanofibrils and cross-linkable xylans for 3D printing. ACS Appl. Mater. Interfaces 9 (46), 40878–40886.
Markstedt, K., Xu, W., Liu, J., Xu, C., Gatenholm, P., 2017. Synthesis of tunable hydrogels based on O-acetyl-galactoglucomannans from spruce. Carbohydr. Polym. 157, 1349–1357.
Masruchin, N., Park, B., Causin, V., 2018. Dual-responsive composite hydrogels based on TEMPO-oxidized cellulose nanofibril and poly (N-isopropylacrylamide) for model drug release. Cellulose 25 (1), 485–502.
Mredha, M.T.I., Na, J.Y., Seon, J., Cui, J., Jeon, I., 2020. Multifunctional poly (disulfide) hydrogels with extremely fast self-healing ability and degradability. Chem. Eng. J. 394, 124941.
Pang, J., Sha, X., Chao, Y., Chen, G., Han, C., Zhu, W., Li, H., Zhang, Q., 2017. Green aqueous biphasic systems containing deep eutectic solvents and sodium salts for the extraction of protein. RSC Adv. 7 (78), 49361–49367.
Paukkonen, H., Kunnari, M., Laurén, P., Hakkarainen, T., Auvinen, V., Oksanen, T., Koivuniemi, R., Yliperttula, M., Laaksonen, T., 2017. Nanofibrillar cellulose hydrogels and reconstructed hydrogels as matrices for controlled drug release. Int. J. Pharm. 532 (1), 269–280.
Paul, S., Sepay, N., Sarkar, S., Roy, P., Dasgupta, S., Sardar, P.S., Majhi, A., 2017. Interaction of serum albumins with fluorescent ligand 4-azido coumarin: spectroscopic analysis and molecular docking studies. New J. Chem. 41 (24), 15392–15404.
Raja, S., Thiruselvi, T., Mandal, A.B., Gnanamani, A., 2015. pH and redox sensitive albumin hydrogel: a self-derived biomaterial. Sci. Rep. 5 (1), 1–11.
Rosendahl, J., Svanström, A., Berglin, M., Petronis, S., Bogestål, Y., Stenlund, P., Standoft, S., Ståhlberg, A., Landberg, G., Chinga-Carrasco, G., 2021. 3D Printed nanocellulose scaffolds as a cancer cell culture model system. Bioengineering 8 (7), 97.
Shi, L., Carstensen, H., Hölzl, K., Lunzer, M., Li, H., Hilborn, J., Ovsianikov, A., Ossipov, D.A., 2017. Dynamic coordination chemistry enables free directional printing of biopolymer hydrogel. Chem. Mater. 29 (14), 5816–5823.
Solin, K., Beaumont, M., Rosenfeldt, S., Orelma, H., Borghei, M., Bacher, M., Opietnik, M., Rojas, O.J., 2020. Self-assembly of soft cellulose nanospheres into colloidal gel layers with enhanced protein adsorption capability for next-generation immunoassays. Small 16 (50), 2004702.
Trombino, S., Servidio, C., Curcio, F., Cassano, R., 2019. Strategies for hyaluronic acid-based hydrogel design in drug delivery. Pharmaceutics 11 (8), 407.
Wang, F., Huang, K., Cao, F., Shi, F., Chen, C., 2022. Self-healable nanocellulose composite hydrogels combining multiple dynamic bonds for drug delivery. Int. J. Biol. Macromol.
Wang, G., Lu, Y., Hou, H., Liu, Y., 2017. Probing the binding behavior and kinetics of silver nanoparticles with bovine serum albumin. RSC Adv. 7 (15), 9393–9401.
Wang, L., Li, L., Wang, X., Huang, D., Yang, F., Shen, H., Li, Z., Wu, D., 2016. UV-triggered thiol–disulfide exchange reaction towards tailored biodegradable hydrogels. Polym. Chem. 7 (7), 1429–1438.
Wang, Q., Xu, W., Koppolu, R., van Bochove, B., Seppälä, J., Hupa, L., Willför, S., Xu, C., Wang, X., 2022. Injectable thiol-ene hydrogel of galactoglucomannan and cellulose nanocrystals in delivery of therapeutic inorganic ions with embedded bioactive glass nanoparticles. Carbohydr. Polym. 276, 118780.
Xia, T., Jiang, X., Deng, L., Yang, M., Chen, X., 2021. Albumin-based dynamic double cross-linked hydrogel with self-healing property for antimicrobial application. Colloids Surf. B: Biointerfaces 208, 112042.
Xu, C., Willfor, S., Sundberg, K., Pettersson, C., Holmbom, B., 2007. Physico-chemical characterization of spruce galactoglucomannan solutions: stability surface activity and rheology. Cellul. Chem. Technol. 41 (1), 51.
Xu, C., Molino, B.Z., Wang, X., Cheng, F., Xu, W., Molino, P., Bacher, M., Su, D., Rosenau, T., Willför, S., 2018. 3D printing of nanocellulose hydrogel scaffolds with tunable mechanical strength towards wound healing application. J. Mater. Chem. B 6 (43), 7066–7075.
Xu, W., Molino, B.Z., Cheng, F., Molino, P.J., Yue, Z., Su, D., Wang, X., Willfor, S., Xu, C., Wallace, G.G., 2019a. On low-concentration inks formulated by nanocellulose assisted with gelatin methacrylate (GelMA) for 3D printing toward wound healing application. ACS Appl. Mater. Interfaces 11 (9), 8838–8848.
Xu, W., Zhang, X., Yang, P., Långvik, O., Wang, X., Zhang, Y., Cheng, F., Österberg, M., Willför, S., Xu, C., 2019b. Surface engineered biomimetic inks based on UV cross-linkable wood biopolymers for 3D printing. ACS Appl. Mater. Interfaces 11 (13), 12389–12400.
Yoon, J.A., Kamada, J., Koynov, K., Mohin, J., Nicolaÿ, R., Zhang, Y., Balazs, A.C., Kowalewski, T., Matyjaszewski, K., 2012. Self-healing polymer films based on thiol–disulfide exchange reactions and self-healing kinetics measured using atomic force microscopy. Macromolecules 45 (1), 142–149.
You, Z., Dong, Y., Li, X., Yang, P., Luo, M., Zhu, Z., Wu, L., Zhou, X., Chen, M., 2021. One-pot synthesis of multi-functional cellulose-based ionic conductive organohydrogel with low-temperature strain sensitivity. Carbohydr. Polym. 251, 117019.
Yu, H., Wang, Y., Yang, H., Peng, K., Zhang, X., 2017. Injectable self-healing hydrogels formed via thiol/disulfide exchange of thiol functionalized F127 and dithiolane modified PEG. J. Mater. Chem. B 5 (22), 4121–4127.
Yue, Y., Li, H., Liu, T., Wu, Y., 2014. Exploring the role of ligand-BSA in the response of BSA-protected gold-nanoclusters to silver (I) ions by FT-IR and circular dichroism spectra. Vib. Spectrosc. 74, 137–141.
Zhang, X., Morits, M., Jonkergouw, C., Ora, A., Valle-Delgado, J.J., Farooq, M., Ajdary, R., Huan, S., Linder, M., Rojas, O., 2020. Three-dimensional printed cell culture model based on spherical colloidal lignin particles and cellulose nanofibril-alginate hydrogel. Biomacromolecules 21 (5), 1875–1885.

Zhang, Y., Sheng, Y., Wang, M., Lu, X., 2022. UV-curable self-healing, high hardness and transparent polyurethane acrylate coating based on dynamic bonds and modified nano-silica. Prog. Org. Coat. 172, 107051.
Zhao, D., Du, Z., Liu, S., Wu, Y., Guan, T., Sun, Q., Ren, B., 2019. UV light curable self-healing superamphiphobic coatings by photopromoted disulfide exchange reaction. ACS Appl. Polym. Mater. 1 (11), 2951–2960.
Zini, J., Kekkonen, J., Kaikkonen, V.A., Laaksonen, T., Keränen, P., Talala, T., Mäkynen, A.J., Yliperttula, M., Nissinen, I., 2021. Drug diffusivities in nanofibrillar cellulose hydrogel by combined time-resolved Raman and fluorescence spectroscopy. J. Control. Release 334, 367–375.
Zong, S., Wen, H., Lv, H., Li, T., Tang, R., Liu, L., Jiang, J., Wang, S., Duan, J., 2022. Intelligent hydrogel with both redox and thermo-response based on cellulose nanofiber for controlled drug delivery. Carbohydr. Polym. 278, 118943.